Small-size microlens characterization by multiwavelength high-resolution interference microscopy

Myun-Sik Kim,* Toralf Scharf, and Hans Peter Herzig

Optics and Photonics Technology Laboratory, Ecole Polytechnique Fédérale de Lausanne (EPFL), Breguet 2, 2000 Neuchâtel, Switzerland
**myunsik.kim@epfl.ch*

Abstract: Microlenses are widely studied in two main areas: fabrication and characterization. Nowadays, characterization draws more attention because it is difficult to apply test techniques to microlenses that are used for conventional optical systems. Especially, small microlenses on a substrate are difficult to characterize because their back focus often stays in the substrate. Here we propose immersion high-resolution interference microscopy to characterize small-size microlenses at three visible wavelengths. Test results for 20-μm-diameter microlenses are presented and discussed. We cover not only standard characterizations like wavefront investigations but also experiments of actual focus properties and chromatic behaviors.

OCIS codes: (120.0120) Instrumentation, measurement, and metrology; (120.4800) Optical standards and testing; (120.5050); Phase measurement; (180.3170) Interference microscopy.

References

1. H. Ottevaere, R. Cox, H. P. Herzig, T. Miyashita, K. Naessens, M. Taghizadeh, R. Völkel, H. J. Woo, and H. Thienpont, "Comparing glass and plastic refractive microlenses fabricated with different technologies," J. Opt. A **8**, S407–S429 (2006).
2. T. Miyashita, "International standards for metrology of microlens arrays," Proc. SPIE **5858**, 585802 (2005).
3. T. Miyashita, M. Kato, and J. Ohta, "Wavefront aberration measurement technology for microlenses using a Mach–Zehnder interferometer with effective apertures," Opt. Eng. **48**(7), 073609 (2009).
4. J. Schwider, and H. Sickinger, "Array tests for microlenses," Optik (Stuttg.) **107**, 26–34 (1997).
5. Y. Li, and E. Wolf, "Focal shifts in diffracted converging spherical waves," Opt. Commun. **39**(4), 211–215 (1981).
6. U. Vokinger, R. Dändliker, P. Blattner, and H. P. Herzig, "Unconventional treatment of focal shift," Opt. Commun. **157**(1-6), 218–224 (1998).
7. C. Rockstuhl, I. Märki, T. Scharf, M. Salt, H. P. Herzig, and R. Dändiker, "High-resolution interference microscopy: a tool for probing optical waves in the far-field on a nanometric length scale," Curr. Nanosci. **2**(4), 337–350 (2006).
8. M.-S. Kim, T. Scharf, and H. P. Herzig, "Amplitude and phase measurements of highly focused light in optical data storage systems," accepted for publication in Jpn. J. Appl. Phys. (2010).
9. D. Malacara, *Opical Shop Testing* (Wiley, 1977), Chap. 2.
10. J. Schwider, R. Burow, K.-E. Elssner, J. Grzanna, R. Spolaczyk, and K. Merkel, "Digital wave-front measuring interferometry: some systematic error sources," Appl. Opt. **22**(21), 3421–3432 (1983).
11. M. Born, and E. Wolf, *Principles of Optics,* 7th ed. (Cambridge Univ. Press, 1999), Chaps. 7 and 9.
12. H. Gross, H. Zugge, M. Peschka, and F. Blechinger, *Handbook of Optical Systems* (Wiley-VCH, 2007) Vol. 3, p. 126.
13. P. Nussbaum, I. Philipoussis, A. Husser, and H. P. Herzig, "Simple technique for replication of micro-optical elements," Opt. Eng. **37**(6), 1804–1808 (1998).
14. H. Sickinger, J. Schwider, and B. Manzke, "Fiber-based Mach–Zehnder interferometer for measuring wave aberrations of microlenses," Optik (Stuttg.) **110**, 239–243 (1999).

1. Introduction

Refractive microlenses and microlens arrays are nowadays common micro-optical elements and have a variety of applications, including basic functions of focusing and collimation. Various fabrication techniques have been developed. Standard techniques lead to plano-

#126342 - $15.00 USD Received 1 Apr 2010; revised 7 Jun 2010; accepted 7 Jun 2010; published 21 Jun 2010

convex lenses, and the fabrication processes require a substrate for the basement of the microlenses [1]. Although there are several standard methods to characterize microlenses [2,3] such as a noncontact optical profiler, Twyman–Green interferometer, and Mach–Zehnder interferometer, they are not always applicable to small-size microlenses, and diffraction disturbs the test of the small-size microlens because of low Fresnel numbers [4]. Interferometry is still the first choice because lenses are tested under operational conditions, which is usually transmission. An interference microscope, which provides magnification to study small-size lenses, leads to a limited number of pixels on a camera sensor, even with high magnifications. Often it gives insufficient data to analyze geometrical and optical characteristics. In tests with sufficiently high magnification, the aberrations caused by the lens geometry, especially the substrate thickness, are often neglected for simplicity [2,3]. If the back focus is in the substrate, an immersion technique will be a valid method to improve the measurement. Moreover, if the lens is not tested at the operation wavelength, chromatic aberration-related phenomena will alter the result. We developed the immersion high-resolution interference microscope (I-HRIM) that allows us to use the highest magnification objectives and that works in immersion at three primary wavelengths in the visible spectrum as a tool for precise measurements of small microlenses on substrates. We have chosen three wavelengths: red at 642 nm, green at 532 nm, and blue at 405 nm.

Another inevitable issue is how to characterize the focal properties. The front focal length, which stays in air, f_{front}, is given as

$$f_{\text{front}} = \frac{\text{ROC}}{(n-1)}, \tag{1}$$

where the radius of the curvature of a lens is ROC and n is the refractive index of the lens material. Small-size microlenses often have the back focal length, f_{back}, inside the substrate. In this case the back focal length is defined as the product of the refractive index of the substrate n_{sub} and the front focal length and reads

$$f_{\text{back}} = n_{\text{sub}} \cdot f_{\text{front}}. \tag{2}$$

When a monochromatic plane wave is focused by a lens and is diffracted at the circular aperture of the lens, the point of the maximum intensity may not coincide with the geometrical focus given in Eqs. (1) and (2). This phenomenon is known as the focal shift [5,6] and the point of maximum intensity is shifted towards the lens. This focal shift depends on the Fresnel number FN which is given as

$$\text{FN} = \frac{\alpha^2}{\lambda f}, \tag{3}$$

where α is the radius of the lens aperture, λ is an operation wavelength, and f is the front or back focal length given in Eqs. (1) or (2), respectively. For large Fresnel numbers, the focal properties of the lens are well described with geometrical optics. For low Fresnel numbers, diffraction influences the focalization properties. In the case of conventional optical systems, which usually have large Fresnel numbers, the focal shift is small and negligible. However, it becomes significant when the Fresnel number is low (≤ 5) [5]. Small-size microlenses have geometrical dimensions that lead usually to low Fresnel numbers because their diameter is small. In the above-mentioned standard interferometric test methods, the measurements of the actual focal properties are not directly achievable because only surface shapes are probed. In order to characterize focal properties, I-HRIM is equipped with a piezo translation stage, which allows moving the sample through a fixed observation plane. By scanning along the optical axis, we can obtain three-dimensional (3D) intensity and phase maps [7,8]. In this paper we use the 3D intensity measurements, which show actual focal properties such as the spot size, effective focal lengths, and depth of focus.

#126342 - $15.00 USD Received 1 Apr 2010; revised 7 Jun 2010; accepted 7 Jun 2010; published 21 Jun 2010

2. Experimental setup and principles of microlens characterization

2.1 High-resolution interference microscopy system setup

High-resolution interference microscopy is already proven as a powerful tool for the characterizations of micro-optics [7,8]. HRIM is working in transmission by employing a Mach–Zehnder type interferometer as shown in Fig. 1(a). Three single-mode polarized laser diodes with different powers and wavelengths are used to create an RGB light source (CrystaLaser 642 nm: DL640-050-3; 532 nm: IR-GCL-025-S; 405 nm: BCL-040-405-S). A polarizing beam splitter (PBS) divides intensities to be sent in a reference and an object arm with adjustable energy ratios. Half-wave plates (HWP) and Glan–Taylor (G–T) polarizers are used to adjust the intensities and to optimize the contrast of the interference fringes. In the object arm, the expanded plane wave illuminates the system under investigation, which is mounted on a precision piezo stage with a z scan range of 500 μm and a nominal accuracy of 1 nm (MAD LAB CITY, NANO Z500). For the spherical wave illumination, we insert an additional objective underneath the sample. Details are given in Section 2.3. We characterize the lens in the pupil plane (the top surface of the substrate of the microlens array) in plane wave and spherical wave illuminations [9]. The z axis piezo stage allows us to precisely find the pupil plane at the highest resolution. In the reference arm, a piezo electrically driven mirror is mounted to change the optical path lengths. The phase distribution of the wave field is obtained by measuring the interference fringes at different mirror positions and employing a classical 5-frame algorithm. In this scheme, 5 frames of the intensity pattern are recorded, each frame being shifted in phase by adding an additional phase of $\lambda / 4$ [10].

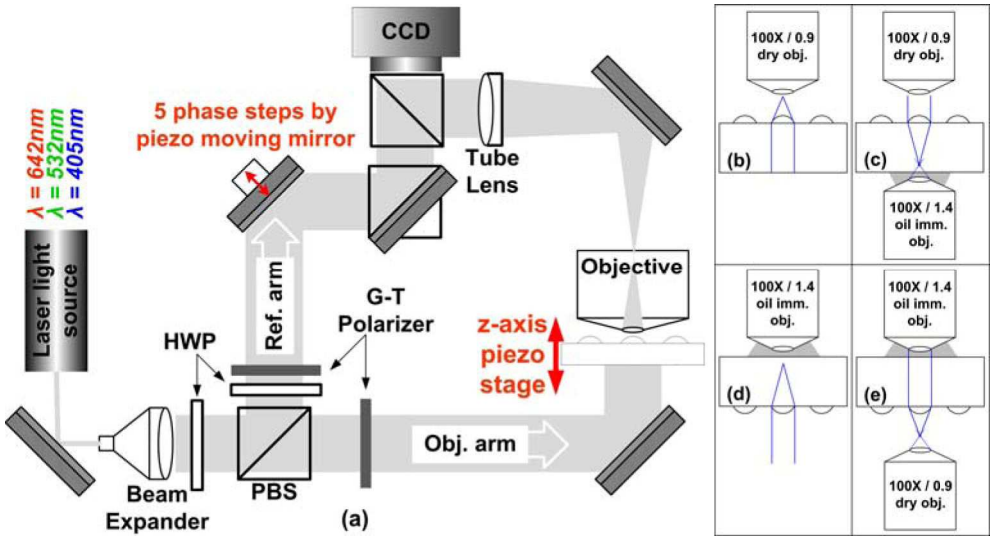

Fig. 1. (a) Schematic of the experimental setup with the plane wave illumination. The piezo stage in the object arm allows one to scan samples with nanometer resolution along the optical axis. In the reference arm, the piezo-driven mirror changes the optical path. Four possible test geometries, (b) the plane wave test and the 3D front focus measurement, (c) the spherical wave test for the back focus, (d) the 3D back focus measurement, and (e) the spherical wave test for the front focus. Gray immersion medium is standard immersion oil for the microscopy.

In general, a high numerical aperture (NA) of the observation objective ensures high resolution of the amplitude and phase measurements. Moreover, high magnification provides more pixels on an image sensor for small fields. We use high NA objective lenses, for example a 100X / NA 0.9 dry objective (Leica Microsystems, HC PL FLUOTAR) and an oil immersion objective with 100X magnification and an NA of 1.4 (Leica Microsystems, HXC PL APO), whose applications are illustrated in Figs. 1(b)–1(e). The objectives are used for both the observation and the illumination, depending on the test geometries. Immersion medium is a standard immersion oil with the refractive index of n_D = 1.515 (Leica

#126342 - $15.00 USD Received 1 Apr 2010; revised 7 Jun 2010; accepted 7 Jun 2010; published 21 Jun 2010

Microsystems, Type N immersion liquid). The resolution of an optical microscope is usually defined as the minimum resolvable distance between two points based on the Rayleigh criterion [11]. The lateral resolutions for the 100X / NA 0.9 objective and the 100X / NA 1.4 objective are 275 nm and 177 nm, respectively, which are calculated with the formula $\Delta x = 0.61\lambda/\mathrm{NA}$ at 405 nm wavelength. Along the optical axis, the Rayleigh criterion can be applied with a simplified formula derived as $\Delta z = \lambda \cdot n/(\mathrm{NA}^2)$ with the refractive index of the immersion medium n [12]. The calculated axial resolutions at 405 nm wavelength are 500 nm for the 100X / NA 0.9 objective in air and 310 nm for the 100X / NA 1.4 objective in immersion oil. At 100X magnification, a pixel on a charge-coupled device (CCD) sensor corresponds to 46.5 nm in the object plane. This leads to the maximum field of view of the CCD camera of 64 µm x 48 µm (Sicon Corporation, CFW1312M camera with SONY ICX205AK image sensor of 1360 x 1024 pixels).

2.2 Plane wave illumination: geometrical properties

Reflow microlenses and their replicas have a convex shape that is considered to be spherical. Such microlenses achieve diffraction-limited quality only at a low NA because a high NA realized with a spherical surface leads to severe spherical aberrations. When such microlenses show a diffraction-limited performance, which means there are practically no aberrations, one can reconstruct a surface profile and geometrical parameters by a transmission plane-wave test. The microlens converts an incident plane wave into a spherical wave, which converges toward its focal point as depicted in Fig. 2. The radius of curvature of the spherical wavefront (R in Fig. 2) defines the focal length *f*. Within the paraxial regime, it agrees well with the theoretical focal length from Eq. (1). The NA is derived from the radius of a lens aperture α and the focal length *f*,

$$\mathrm{NA} = \frac{\alpha}{f}. \tag{4}$$

For small aberrations one can retrieve the surface profile and obtain the lens shape parameters such as sag height, radius of curvature, and diameter of the lens.

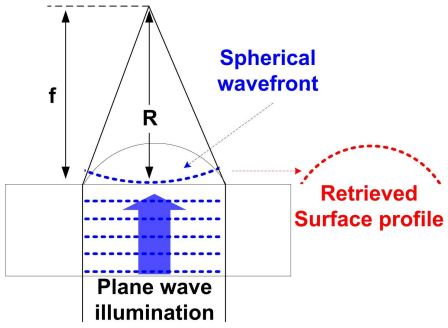

Fig. 2. Plane-wave illumination: measurement of spherical wavefront provides the geometrical properties and the surface profile of the lens.

2.3 Spherical wave illumination: optical properties and quality parameters

Lenses can be tested for their focus properties with spherical wave illumination. The microlens collimates an incoming spherical wave and transforms it in the ideal case into a plane wave when the focal point of the spherical wave is brought into the back focus of the microlens. The wavefront errors are obtained by comparing the measured wavefront emerging from the microlens with an ideal plane wave. The lens quality is acceptable when the Maréchal Criterion for diffraction-limited lenses is fulfilled (RMS wavefront error < 0.07λ and Strehl ratio > 0.8) [11]. More detailed parameters such as Zernike coefficients can be retrieved from such measured wavefront data. As seen in Fig. 3, the back focal point might be

#126342 - $15.00 USD Received 1 Apr 2010; revised 7 Jun 2010; accepted 7 Jun 2010; published 21 Jun 2010

outside or inside the substrate. If the focal point stays inside the substrate the refraction at the interface between air and the bottom substrate surface causes aberrations, as shown in Fig. 3(b). Figure 3(c) shows that the immersion scheme, which immerses the space between the illuminating objective and the substrate, allows avoidance of refraction. The influence of this effect becomes significant when the NA of lenses under testing is large and the substrate is thick. An example of such a situation is shown in Fig. 4(a). Two measurements for the same lens are shown. Figure 4(a) is done in test geometry as in Fig. 3(b), and Fig. 4(b) is done in immersion, where the influence of refraction at the substrate surface is eliminated. The fringe images already show severe differences and justify the use of the immersion technique. For high-quality measurement it is therefore necessary to avoid refraction and aberration from the substrates.

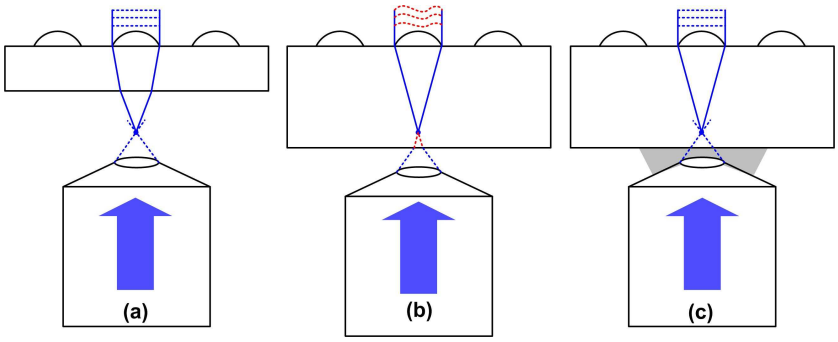

Fig. 3. Spherical wave illumination: the lens converts an incoming spherical wave into a plane wave. (a) The back focus stays outside the substrate. (b) The back focus stays inside the substrate and refraction at the bottom surface causes aberrations. (c) The immersion in the illumination suppresses refraction at the lower substrate surface.

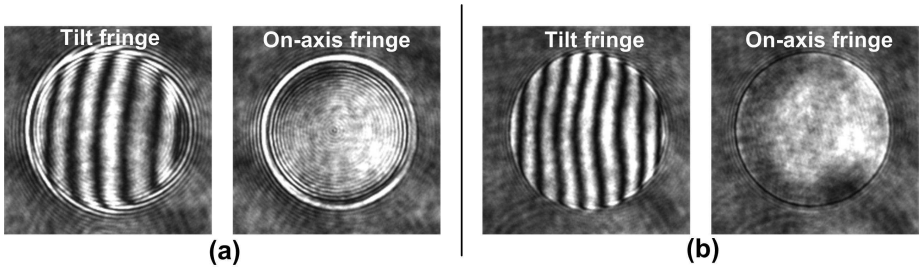

Fig. 4. Example shows influence of immersion on lens testing. The sample lens has a diameter of 62 µm, an NA of 0.43, and a back focal length of 100 µm, which stays in the substrate of 170 µm thickness. Spherical wave illumination is used according to Figs. 3(b) and 3(c)—in (a) a 100X / NA 0.9 dry objective is used, and in (b) 100X / NA of 1.4 oil immersion objective is used.

3. Characterization of a 20 µm diameter microlens at different wavelengths

3.1 Test sample

We fabricated microlens arrays by a replication technique [13]. The diameter is 20 µm, and they are arranged in an array of a 22 µm pitch. Since the working distance of the immersion objective is adapted to microscopic cover-glass thickness of usually 170 µm, such a cover glass is used as a substrate for replication. Norland optical adhesive NOA 61 is applied as the replication material and has a refractive index of 1.58 at wavelength 405 nm, 1.565 at 532 nm, and 1.556 at 642 nm. A scanning electron microscope (SEM) image of the replicated microlens array is shown in Fig. 5. It demonstrates the uniformity of fabricated microlenses.

#126342 - $15.00 USD Received 1 Apr 2010; revised 7 Jun 2010; accepted 7 Jun 2010; published 21 Jun 2010

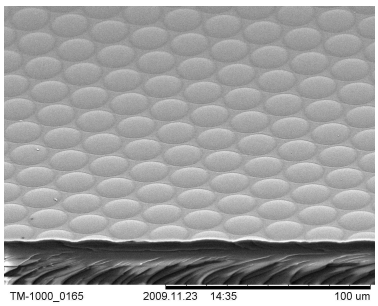

Fig. 5. SEM image of replicated polymer microlens array with 20 µm diameter and 22 µm pitch at a 45° inclination angle.

3.2 Plane wave test

Typical interferometer fringe images of microlenses and measured wrapped phase images are shown in Fig. 6. An image size of 440 x 440 pixels represents a field of 20 µm x 20 µm, which corresponds to the lens aperture. Although the fringe contrast of the measurement at different wavelengths differs, the final results are not altered. The fringe contrast is very much dependent on the quality of the components and their achromatic correction. In Section 3.4 analyses of these measurements will be discussed in more detail.

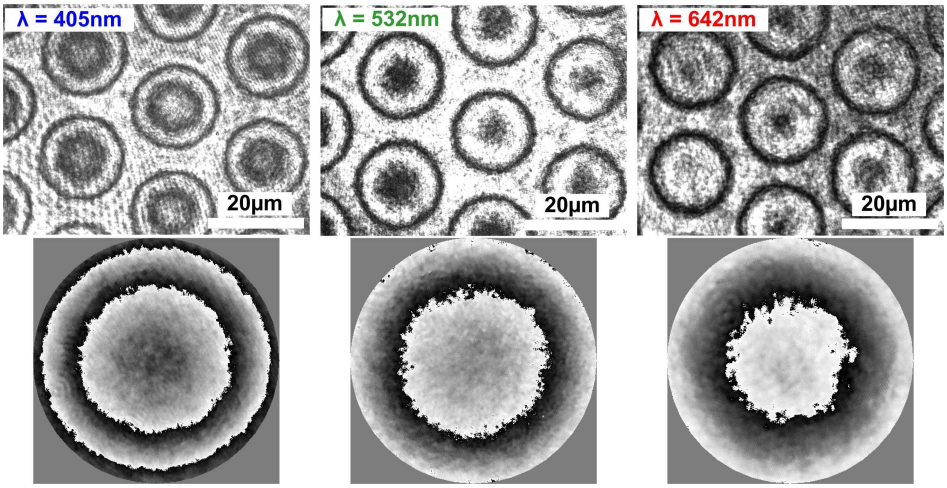

Fig. 6. Interferometric fringe images of microlens illuminated with a plane wave: full field of view of the CCD camera (upper row) and measured wrapped phase within the lens aperture (bottom row) for 405 nm (left), 532 nm (center), and 642 nm (right).

3.3 Spherical wave test

Since the back focus of the test lens lies inside the substrate, the immersion scheme is applied to illuminate the microlens with a spherical wave, as shown in Fig. 3(c). The lens under test transforms an incoming spherical wave into a plane wave and the lens quality is measured differentially. Figure 7 shows full-field fringe images and measured wavefronts within the lens aperture. The high quality of the measurements allows us to determine even the smallest aberrations. For numerical apertures smaller than 0.17 (paraxial limit), a spherical plano-convex microlens can show diffraction-limited performance, which is experimentally verified in Fig. 7. For three wavelengths, RMS wavefront errors are found to be below 0.02λ leading to a Strehl ratio over 0.98. Although the spherical aberration is small for the test lens, the front focus is expected to show larger aberration owing to higher refractive power than the back focus. This can be demonstrated by illuminating a spherical wave through the front focus. For three wavelengths, full-field fringe images and measured wavefronts within the lens aperture

#126342 - $15.00 USD Received 1 Apr 2010; revised 7 Jun 2010; accepted 7 Jun 2010; published 21 Jun 2010

are shown in Fig. 8. In this case, RMS wavefront errors are found to be approximately 0.04λ. As expected, it shows slightly larger wavefront errors due to the spherical aberration caused by inappropriate orientation of the plano-convex lens.

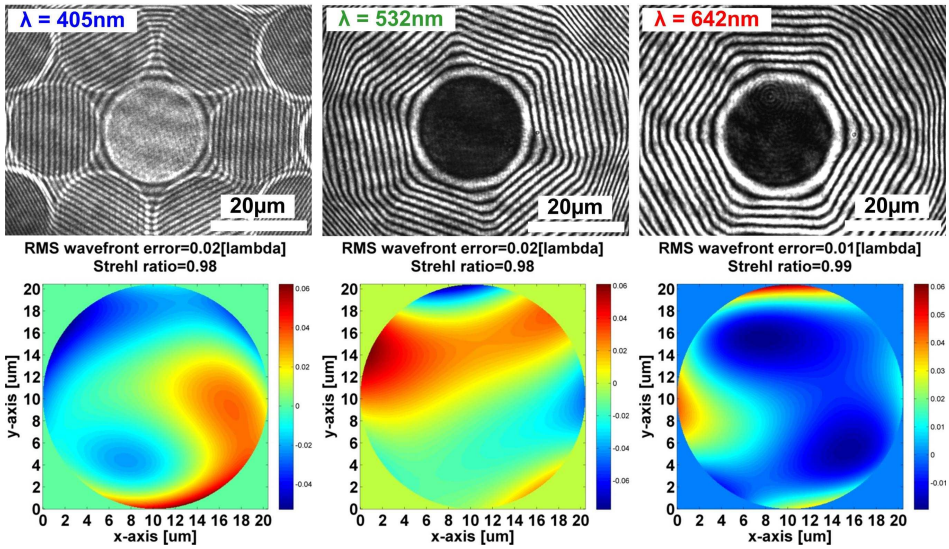

Fig. 7. Interferometric fringe images of a microlens illuminated with a spherical wave through its back focus: full-field view of the CCD camera (upper row) and measured wavefront deviations from a plane wave within the lens aperture (bottom row) for 405 nm (left), 532 nm (center), and 642 nm (right).

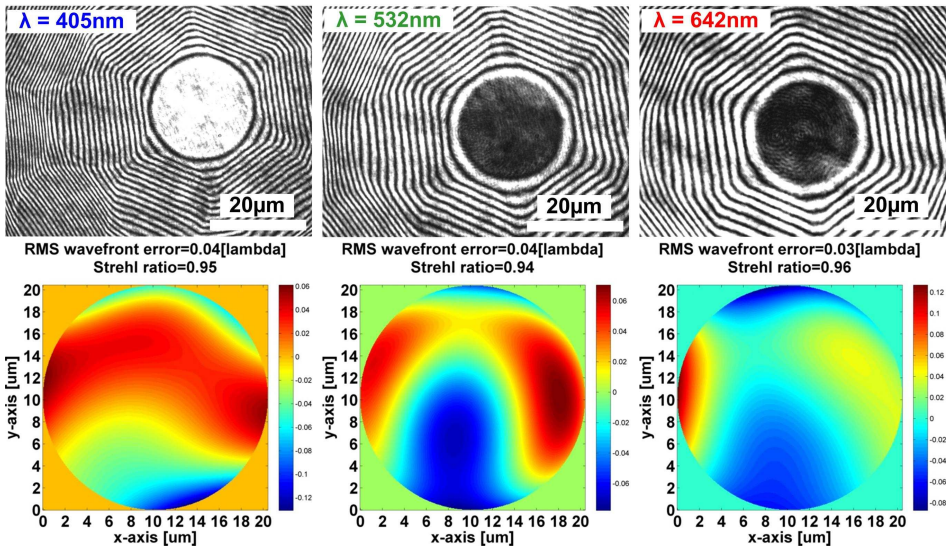

Fig. 8. Interferometric fringe images of microlens illuminated with a spherical wave through its front focus: full-field of view of the CCD camera (upper row) and measured wavefront deviations from a plane wave within the lens aperture (bottom row) for 405 nm (left), 532 nm (center), and 642 nm (right).

A shorter wavelength generates narrower fringes, as observed in Figs. 6, 7, and 8. However, there are no substantial changes in the optical properties depending on the wavelength because the test lens has a low NA and diffraction-limited performance.

#126342 - $15.00 USD Received 1 Apr 2010; revised 7 Jun 2010; accepted 7 Jun 2010; published 21 Jun 2010

3.4 Reconstruction of surface profile

In the previous section we verified that our lens has diffraction-limited performance and nearly no aberrations. As discussed in Section 2.2, we can reconstruct the surface profile and geometrical parameters by phase unwrapping of the plane wave measurements. We compare these measurements done for different wavelengths with direct surface shapes obtained with a WYCO NT330 optical profiler. Results are shown in Fig. 9. The material dispersion is corrected in the geometrical shape analysis. It shows exactly the same geometry for the three wavelengths, a ROC of 37 μm, and a sag height of 1.4 μm. RMS deviations from the surface profile are below 0.05λ for all three wavelengths. The front focal length f_{front} and numerical aperture NA are calculated by using Eqs. (1) and (4) and are summarized in Table 1. Although the shape parameters are the same for the three different wavelengths, the focal length and the NA slightly vary because of dispersion.

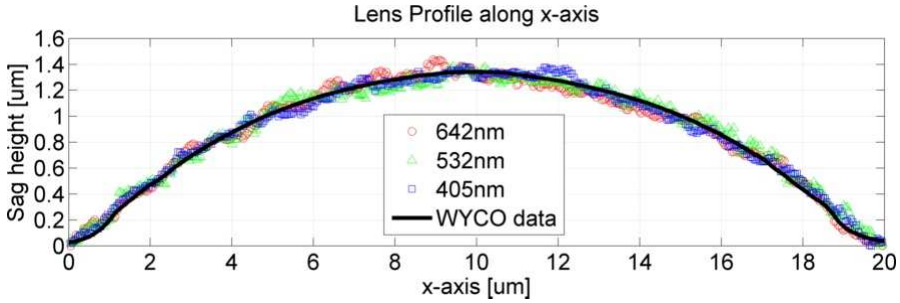

Fig. 9. Retrieved surface profiles from measured wavefronts for 405 nm (red square), 532 nm (green triangle), 642 nm (blue square), and the measured profile by the WYCO NT3300 optical profiler (black line).

Table 1. Geometrical Parameters by Plane Wave Test for Three Wavelengths

	Wavelength		
	405 nm	532 nm	642 nm
Refractive index of NOA 61	1.580	1.565	1.556
ROC	37 μm	37 μm	37 μm
Sag height	1.4 μm	1.4 μm	1.4 μm
Calculated front focal length	63.8 μm	65.5 μm	66.5 μm
Calculated numerical aperture	0.156	0.152	0.150
Fresnel number	3.9	2.9	2.3

4. Exprimental evaluation of focussing properties

As we have shown in the previous section, there are no differences in the geometrical characteristics and quality when the microlenses are characterized at three different wavelengths. This is because of the low numerical aperture and the low dispersion. However, the focal characteristics, such as the spot size and the depth of focus, are directly related to the operation wavelength and should lead to remarkable differences. To explore these parameters, the actual focuses are experimentally studied by scanning the emerging light field along the optical axis with the I-HRIM. The HRIM allows us to obtain the intensity and the phase fields. Phase measurements as shown in inset in Fig. 10 remain unspecific. For low NA lenses, the intensity measurements contain more specific information as compared to the phase-field measurements. 3D intensity maps are recorded for front and back focus measurements, and the *x*-*z* slices are shown in Figs. 10 and 11, respectively.

#126342 - $15.00 USD Received 1 Apr 2010; revised 7 Jun 2010; accepted 7 Jun 2010; published 21 Jun 2010

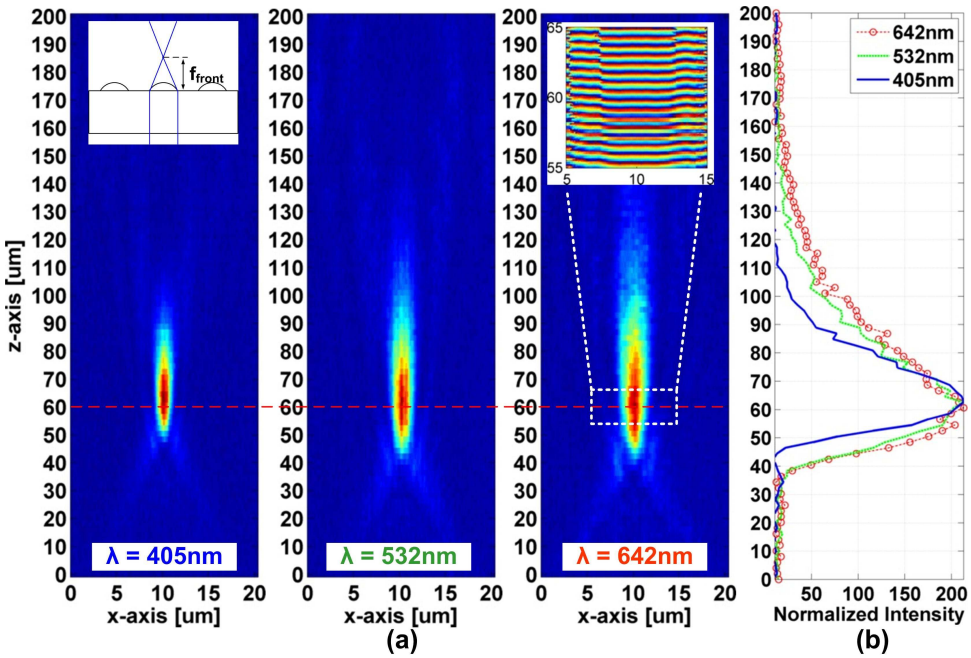

Fig. 10. Measured 3D intensity map of the front focus: (a) the *x*-*z* slices for 405 nm (left), 532 nm (center), 642 nm (right), and (b) on-axis intensity profiles of three wavelengths. The substrate surface and the lens rim are located at position 0 on the *z* axis. A typical phase measurement is displayed in the inset of the 642 nm intensity map.

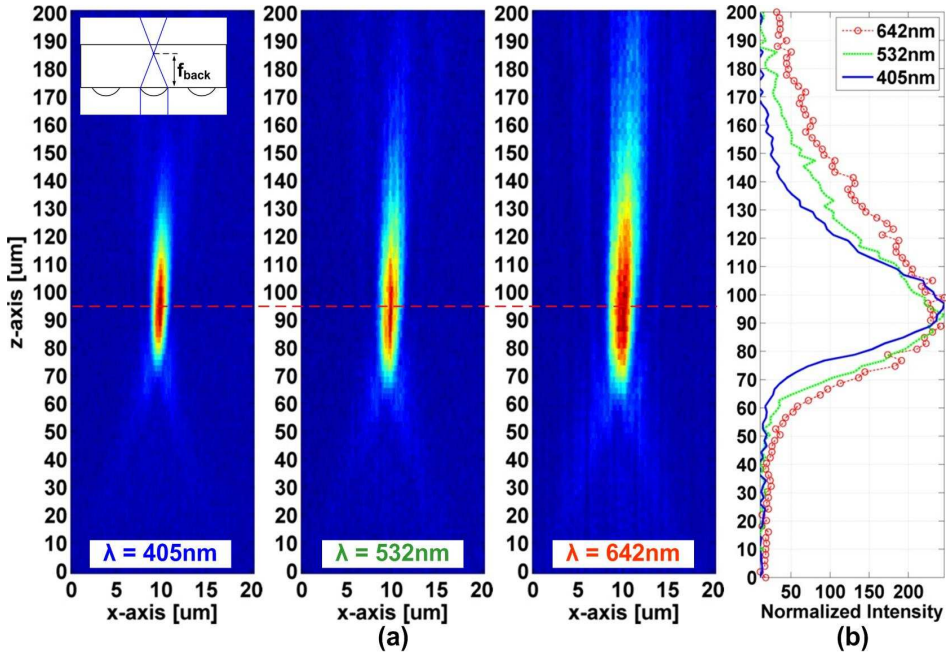

Fig. 11. Measured 3D intensity map of the back focus: (a) the *x*-*z* slices for 405 nm (left), 532 nm (center), 642 nm (right), and (b) on-axis intensity profiles of three wavelengths. The substrate surface and the lens rim are located at position 0 on the *z* axis.

The focal point that determines the experimental focal length is obtained as the point of maximum on-axis intensity. The front focal length is measured at approximately 62 μm for

#126342 - $15.00 USD Received 1 Apr 2010; revised 7 Jun 2010; accepted 7 Jun 2010; published 21 Jun 2010

three wavelengths. For the back focus, which stays inside the substrate, an immersion objective is used. The back focal length is experimentally found as approximately 95 μm for all three wavelengths. The measured focal lengths stay in the vicinity of theoretical values from Eqs. (1) and (2).

4.1 Spot size

In order to verify the spot size, the measured width of the Airy disc at FWHM is compared with theoretical values. For the experimental convenience, we use a FWHM as the experimental spot size, and the theoretical one is derived from wavelength λ and the NA as

$$\mathrm{FWHM}_{\mathrm{spotsize}} = 0.5\frac{\lambda}{\mathrm{NA}}. \tag{5}$$

Table 2 gives the spot sizes for all wavelengths. The experiments agree well with the theoretical values. Figures 10 and 11 show the wavelength dependence, and as expected a shorter wavelength leads to a smaller spot size. The focal length varies depending on the focal side when the back focus stays in the substrate. On the contrary, the spot size is the same for either focal side. In order to understand it, we rewrite Eq. (4) as the product of the refractive index of the medium *n* and the half-angle of the maximum cone of light θ,

$$\mathrm{NA} = n \cdot \sin(\theta). \tag{6}$$

When the paraxial lens has the back focus in the substrate, sin(θ) is defined as α/(*n*·*f*). Since the refractive index of the medium n is imbedded as a denominator in sin(θ), *n* is finally canceled in Eq. (6). The NA remains the same. Consequently Eq. (5) provides the same spot size at the same wavelength independent for both focal sides.

Table 2. Theoretical and Experimental Spot Sizes for Three Wavelengths

	Wavelength		
	405 nm	532 nm	642 nm
Theoretical $\mathrm{FWHM}_{\mathrm{spotsize}}$	1.3 μm	1.8 μm	2.1 μm
Experimental FWHM of front focus	1.3 μm	1.8μm	2.3μm
Experimental FWHM of back focus	1.3 μm	1.8 μm	2.4 μm

4.2 Depth of focus

There are several representations for the depths of focus (DOF). The DOF is usually used as a measure to estimate the tolerance of the positioning of the image plane in relation to the lens or to determine the axial resolution of the lens. The wave optical depth of focus can be defined as the distance, where the intensity on the optical axis has fallen to 80% [12]:

$$\mathrm{DOF} = \frac{\lambda \cdot n}{\mathrm{NA}^2}. \tag{7}$$

In this formula, the refractive index *n* is usually taken in the image space, where the depth of focus should be considered. From on-axis intensity profiles, we can pick up an experimental counterpart of the theoretical DOF, which is the distance where the peak intensity has decreased to 80%. The theoretical and experimental depths of focus are listed in Table 3 for the front and back focus. While the NA stays the same on both focal sides, the refractive index varies. The front focus has a smaller DOF than the back focus because the front focus lies in air ($n_{\mathrm{air}} = 1$). Referring to Tables 2 and 3 and comparing Figs. 10 and 11, it is clearly observed that axial spots become larger for the back focus, whereas the lateral spot sizes do not change for the same wavelength.

#126342 - $15.00 USD Received 1 Apr 2010; revised 7 Jun 2010; accepted 7 Jun 2010; published 21 Jun 2010

Table 3. Theoretical and Experimental Depth of Focus for Three Wavelengths

		Wavelength		
		405 nm	532 nm	642 nm
Front focus	Theoretical DOF	16 µm	24 µm	29 µm
	Experimental DOF	16 µm	19 µm	24 µm
Back focus	Theoretical DOF	24 µm	36 µm	43 µm
	Experimental DOF	22 µm	24 µm	31 µm

5. Conclusions

We proposed, for the first time to our knowledge, a new immersion high-resolution interference microscopy (I-HRIM) technique working at several wavelengths to characterize small-size microlenses. Our approach is particularly interesting for cases when the back focus stays in the substrate. The instrument is equipped with red, green, and blue laser sources to cover the visible spectrum. The possibility of working in immersion allows higher resolution and avoidance of measurement-related aberrations during the focus characterization when observation and illumination are done through the substrate. We demonstrated the performance by measuring small-size microlenses replicated on a 170-µm-thick glass substrate. The lenses have a 20 µm diameter and a 22 µm pitch. The results of the plane-wave and spherical-wave tests confirm reliable performances of optical and geometrical characterizations at all wavelengths. Since the test lenses have a relatively low numerical aperture, experimental parameters are discussed within the paraxial approximation and show a good agreement with theory. The actual focal properties were experimentally studied by using the 3D scanning function of the I-HRIM. While the phase measurement shows little analytical information for low NA lenses, the 3D intensity measurements reveal the wavelength dependence of spot size and the depth of focus (DOF). Our results confirm the capability of RGB immersion HRIM to study optical wave fields at very high precision.

Acknowledgement

We thank SUSS MICROOPTICS (http://www.suss-microoptics.com) for providing us with microlenses. The research leading to these results has received funding from the European Community's Seventh Framework Programme FP7-ICT-2007-2 under grant agreement 224226.

#126342 - $15.00 USD Received 1 Apr 2010; revised 7 Jun 2010; accepted 7 Jun 2010; published 21 Jun 2010